A Modular Sensor Suite for Propulsion Testing

Yudaya Sivathanu[1], Jongmook Lim, Marcus Wolverton, Vinoo Narayanan, and Jason Green

En'Urga Inc.
1201 Cumberland Avenue, West Lafayette, IN 47906

Abstract

Industrial process tomography is widely used for the characterization of a wide variety of physical processes. One of the drawbacks of process tomography equipment is that they are specific to a particular application and process. Therefore, different instruments are required for characterizing turbulent sprays and flames. A modular sensor suite is developed to characterize flames and sprays used in the propulsion industry. The sensor suite enables the user to select from a range of plug and play emitter and sensor modules to estimate several physical characteristics of the system under study. The sensor suite developed in this study is capable of measuring planar temperatures, radical species concentrations (such as OH, AlO, CH, C+), and particulate volume fractions in flames and planar surface area densities and drop sizes in sprays. The modular suite also has a configurable algorithm with an embedded database that includes many of the radiative properties, such as wavelength and line width, gas species, and particulate volume fractions. The sensor suite is a monolithic structure that can be mounted in any orientation around the physical process. Sample soot and temperature data from ethylene and propulsion diffusion flames ,and OH concentrations from a hydrogen flame are presented to highlight the capabilities of the sensor suite in characterizing turbulent diffusion flames. In addition, sample surface area densities and drop sizes from a water spray are presented to highlight the capability of the sensor suite to characterize sprays. The data obtained from the sensor suite is validated using data from published literature for flames and using Phase Doppler Interferometry in sprays. The current sensor suite can accommodate flames and sprays that are up to 250 mm in diameter, making it a valuable diagnostic for the propulsion industry.

Keywords

Rocket and Aircraft Propulsion System Diagnostics, Absorption Tomography, Emission Tomography, Planar Temperature Measurement, Planar soot volume fractions, Planar drop sizes

Introduction

Recently, Ehn et al. (2017) reviewed advanced laser-based techniques for gas-phase diagnostics in reacting flows. The principle methods for obtaining planar information in reacting and non-reacting flows include Planar Laser-Induced Fluorescence (Zhou et al., 2015), Particle Image Velocimetry (Alkislar et al., 2000), two-color thermometry (Brisley et al., 2005), Coherent anti-Stokes Raman Scattering (Bohlin and Kliewer, 2015), chemiluminescence (Floyd et al., 2011), Fan Beam Emission Tomography (Sivathanu et al., 2007) Tunable Diode Laser Absorption Spectroscopy (Xu et al., 2016) and Particle Imaging Velocimetry (Alkislar et al., 2003), Pattern Imaging Velocimetry (Sivathanu et al., 2019) and Statistical Extinction Tomography (Lim et al., 2003). Besides there are several other methods not mentioned here used in a wide variety of flows.

Using the above diagnostic methods, we can obtain planar temperatures, major and minor species concentrations, particulate volume fractions, drop surface area densities, drop sizes, and velocities. Most of these techniques require custom hardware and software that apply to only that technique. For instance, you would use two-color thermometry for obtaining planar temperatures,

[1] Corresponding author: sivathan@enurga.com
Distribution Level: A

without concentration information. Or you could use extinction tomography to acquire particle drop surface areas. If you desire to receive multiple details, you could use some of the spectroscopic techniques (such as TDLAS, FBET) that provide concentrations and temperatures. Even this information is limited to a certain extent by choice of wavelengths used for the spectroscopic measurements.

Based on the above, the primary objective of this study is to develop a modular sensor suite that can be configured to obtain different information in turbulent reacting and non-reacting flows. The sensor suite is populated with receiving modules and sending modules. The intent is to create a plug and play approach using these receiving and sending modules to measure various properties using a common platform.

Experimental Arrangement

The frame of a circular extinction-based optical patternator is utilized as a general-purpose platform. A solid model of the sensor suite is shown in Fig. 1.

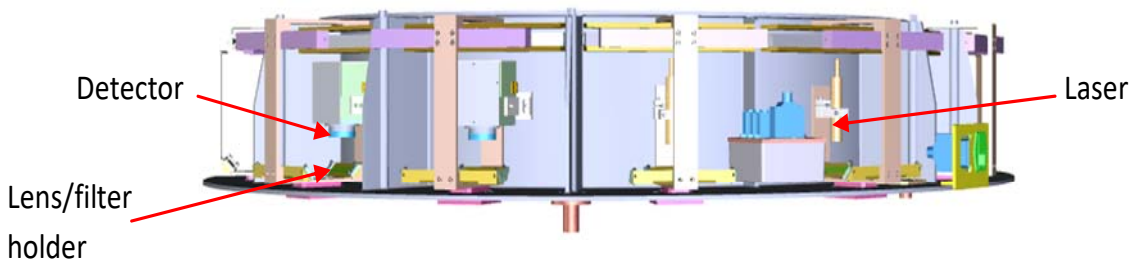

Figure 1. Solid model of the sensor suite.

A sensor suite contains a fixed number of receiving and/or transmitting optical modules, arranged in a dodecagon (twelve-sided polygon) pattern as shown in Fig. 2.

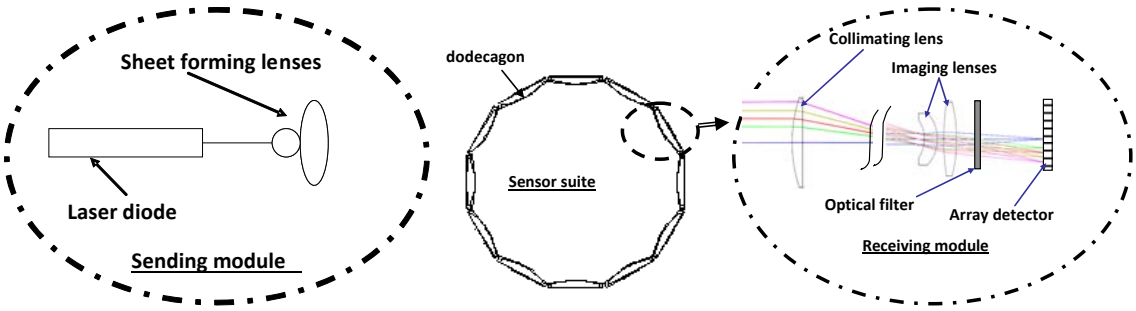

Figure 2. Schematic of the modular sensor suite.

The two critical elements of the modular sensor suite are the radiation receiving and radiation transmitting modules. The radiation sending module is shown on the left panel of Figure 2, the sensor suite is shown in the middle panel, and the receiving module is shown on the right panel of Figure 2. The sending module consists of a laser and sheet forming optics. The laser sheet typically has a fan beam collimated by the collimating lenses shown in the sensor suite (middle of Fig. 2).

The receiving module consists of three sub-elements, i.e., the lenses, the filter, and the array detector. The collimating lens (shown on the figure of the sensor suite as well as separately in the exploded view) is the first element and is used to ensure that only parallel rays enter the array detector. The diameter of the collimating lens determines the size of the flame/spray that can be interrogated

with the system. For the work presented here, the diameter of the interrogated area is 175 mm. The platform for the sensor suite had an internal diameter of 875 mm and an external diameter of 1225 mm.

The imaging lenses are used to focus the radiation from the flame (for emission measurements) or the sending optics (for extinction measurements) onto the linear array. The second element is a filter. The filter used depends specifically on the species that is being studied. For example, a filter centered at 313 nm can be used to study OH chemiluminescence. In this study, the primary focus is on determining soot volume fractions in the overfire region using extinction tomography, and soot volume fractions and temperatures in the underfire region using emission tomography.

A photograph of the sending and receiving modules are shown in Fig. 3.

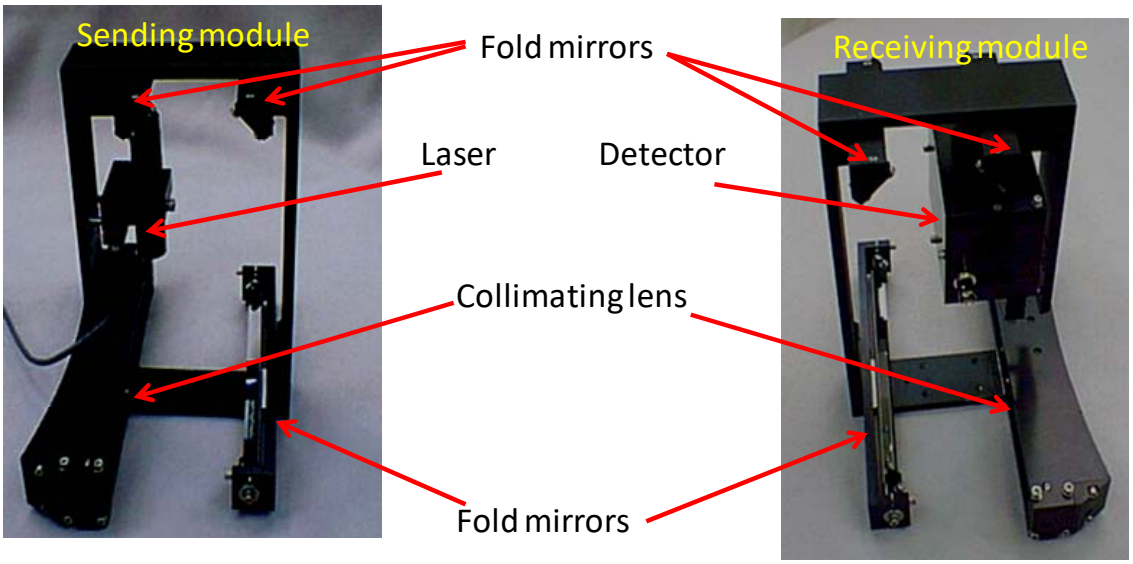

Figure 3. Photograph of the sending and receiving modules.

Both the sending and receiving units are identical in footprint. The sending module typically has a laser and the collimating lens, while the receiving unit has the collimating lens and the detector unit. Fold mirrors are used to reduce the footprint of the instrument.

Numerical Methods

The deconvolution algorithm used with these modules is described first. Only four modules are discussed in the following. The first module is for estimating soot volume fractions from extinction measurements at 632 nm. The second module determines temperatures and soot volume fractions from two-wavelength emission measurements at 800 and 900 nm. The third module is for estimating local OH emission intensities from chemiluminescence measurements at 310 nm. The last module is for estimating drop surface area densities and drop Sauter Mean Diameter (SMD) from combined extinction and scattering measurements at 635 nm. The four modules are described in further detail below.

Soot Volume Fraction Module

The extinction measurements are first deconvoluted using the Maximum Likelihood Estimation (MLE) method of Vardi and Lee (1993). The details of the method for determining local extinction from the path integrated measured will be discussed first. The modular suite provides the path integrated transmittances (T_j^i)along the 512 parallel paths (i) and for six axes or view angles (j). The local extinction coefficients are obtained from the transmittance measurements by deconvolution. The

division of the domain into homogeneous sections (concentric arcs subtending 30 degrees at the center with a width of approximately 0.75 mm) for the deconvolution problem being considered is shown in Fig. 4. The flame or particulate flow within the domain is assumed to be turbulent and stationary. Axi-symmetry is not assumed for the flame or the particulate flow. The instantaneous transmittance and temperature of each ring fluctuate with time. However, the assumption of a stationary turbulent flow implies that the moments of transmittance (time-averaged) are constant and homogeneous for each path. The interrogation domain is divided into twelve pie-shaped zones and 512 concentric circles.

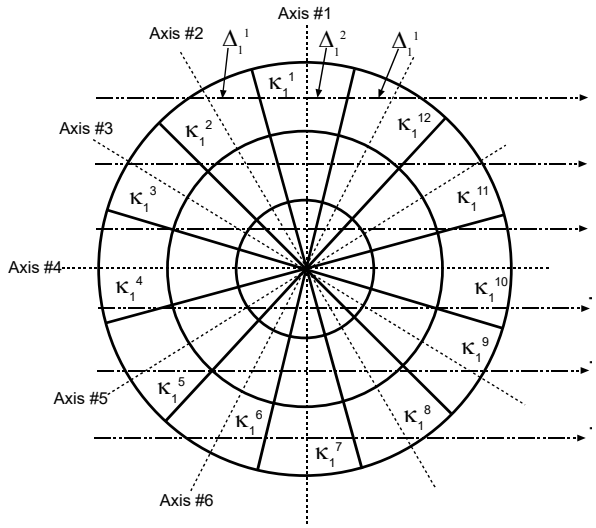

Figure 4. A schematic of the deconvolution domain for the sensor suite.

Therefore, there is a total of 3072 homogeneous sections in the deconvolution domain. The dotted lines in Fig 4. show the six axes or view angles of the sensor suite. The path integrated transmittances that are measured for six representative parallel paths for the first view angle (axis #1) are shown as T_1^1 to T_1^6 in Fig. 4.

It should be noted that the local extinctions coefficients along axis #1 are obtained from the transmittance measurements conducted perpendicular to axis #1. In each section, the specific extinction coefficient (κ_i^j) is assumed to be homogeneous, where i represents the concentric circle, and j represents the zone (not the view angle since the deconvolution domain can be split into greater than six zones (Lim and Sivathanu, 2005). This is the basic spatial resolution of the system. For the light path 1 in Fig. 2, the instantaneous path-integrated transmittance can be related to the local extinction coefficients of the sections through which the light path passes as:

$$\exp(-\kappa_1^1\Delta_1^1 - \kappa_1^2\Delta_1^2 - \kappa_1^3\Delta_1^1) = I_1{}^1 \tag{1}$$

where the Δ_i^j represents the path length traversed by the beam in the ith circle and j^{th} zone. Eq. 1 can be rewritten as a linear equation by using the logarithm function as follows:

$$\kappa_1^1\Delta_1^1 + \kappa_1^2\Delta_1^2 + \kappa_1^3\Delta_1^1 = -\log(I_1{}^1) \tag{2}$$

Similarly, linear equations can be constructed from the optical paths for the remaining 5 axes.

There is a total of 6 x 512 optical paths available from the measurements. The total number of unknown variables, κ_i^j is 256x12. The first moment (mean) of the extinction coefficient, κ_i^j can be written as:

$$E\left\{\kappa_1^1\Delta_1^1 + \kappa_1^2\Delta_1^2 + \kappa_1^3\Delta_1^1\right\} = E\left\{-\log\left(I_1{}^1\right)\right\} \tag{3}$$

Equation 3 is a linear equation and therefore, the averaging operation can be carried separately for the terms as follows:

$$\Delta_1^1 E\left\{\kappa_1^1\right\} + \Delta_1^2 E\left\{\kappa_1^2\right\} + \Delta_1^1 E\left\{\kappa_1^3\right\} = E\left\{-\log\left(I_1{}^1\right)\right\} \tag{4}$$

The optical path lengths, Δ_i^j, are constant and can be calculated from the geometry of the problem. The first moments (mean) of the path-integrated transmittances, $E\left\{-\log\left(I_1{}^i\right)\right\}$, are obtained from the measurements. By taking the expectation operator for all 512 optical paths and six axes, a linear system of equations for mean local extinction coefficients for the 3072 homogeneous sections can be constructed. The constructed system of linear equations for the mean of the local extinction coefficients are inherently ill-conditioned and have a positive coefficient matrix. Furthermore, the solution must be positive because the extinction coefficients are always positive. The MLE method (Vardi and Lee, 1993) is best suited for handling linear inverse problems with positivity constraints, due to its guaranteed convergence and ease of implementation. The MLE method converges to an optimal solution with log norm for both square and non-square matrices. The solution of the equations provides the local mean extinction coefficients across the entire plane in the deconvolution domain. The algorithm has already been tested in the past with synthetic data as well as with water sprays (Lim and Sivathanu, 2005).

After the mean local extinction coefficient is calculated, the soot volume fraction can be obtained, using the Rayleigh approximation, as:

$$f_V = \frac{\ln(-\kappa_i^j).\lambda}{H_\lambda \Delta_i^j} \tag{5}$$

where f_V is the local soot volume fraction, and H_λ is the dimensionless extinction coefficient obtained from the refractive indices of soot at the wavelength, λ (Siegel and Howell, 1992) and a value of 9.3 (average value from Williams et al., 2006) is used in these experiments.

This dimensionless constant provides the local soot volume fractions from the absorption measurements. The above set of equations can also be used to solve for any non-radiating material in the path of the laser sheet (such as jet exhaust particulates, cold sprays, etc.)as long as the refractive indices of the material are known.

Temperature Module

The second module that is developed is the soot temperature module. To determine the temperatures in a plume, the emissivity is required. A two-wavelength technique is used for estimating temperatures and emissivity simultaneously (Sivathanu and Faeth, 1990). For emission tomography at two wavelengths, the spectral radiation intensity, I_λ emitted by a small segment in the flame at any wavelength λ, is given by the Radiative Transfer Equation (RTE) as:

$$I_\lambda = I_{b\lambda}.(1 - \exp(-H_\lambda f_V \Delta/\lambda)) \tag{6}$$

where $I_{\lambda b}$ is the Planck function (dependent on the temperature only), H_λ is a function of the real and imaginary refractive indices of soot (Siegel and Howell, 1992), f_v is the local soot volume fraction, and Δ is the optical path length. The spectral radiation intensity (by using the definition of black body radiation) can, therefore, be written as:

$$I_\lambda = 2\pi \frac{hc^2}{\lambda^5} . \frac{1}{\exp(hc/\lambda kT)} .(1 - \exp(-H_\lambda f_v \Delta / \lambda)) \tag{7}$$

where h, c, and k are the fundamental radiation constants. For a given temperature and soot volume fraction, the spectral emission intensity along the optical path can be calculated using the equation of radiative transfer shown in Eq. 7.

The path integrated emission I_λ^i, for the path i, can be obtained as:

$$I_\lambda^i = \sum_{k=1}^{N} I_{b\lambda}^k .[T_{1\lambda} . T_{2\lambda} .....T_{k\lambda}].[1 - \exp(H_{k\lambda} . f_v . \Delta_k / \lambda)] \tag{8}$$

where N is the number of optical path segments along the line of sight for the given optical path and $T_{k\lambda}$.is the spectral transmittance along the path Δ_k. When Eq. (8) is solved using the MLE method, the local intensity measurement will be available at any wavelength. For emission tomography, the path integrated intensities are measured at two different wavelengths, and the local intensities obtained from the deconvolution procedure. These local intensities at two wavelengths are used to estimate the temperature (Sivathanu and Faeth, 1990b). Using Eq. (7) and the deconvoluted local intensities at two wavelengths, the temperature is obtained as:

$$T = \frac{hc}{k} .(\frac{1}{\lambda_1} - \frac{1}{\lambda_2}) / \ln[(\frac{I_{\lambda 1}}{I_{\lambda 1}})(\frac{\varepsilon_{\lambda 1}}{\varepsilon_{\lambda 2}})(\frac{\lambda_2}{\lambda_1})^5] \tag{9}$$

where $\varepsilon_{\lambda 1}$ is the emissivity of the segment and is equal to $1-K_1$.

The temperature module also uses the dimensionless extinction coefficient of 9.3 (Williams et al., 2006) as the radiating species is soot. The soot volume fraction and temperature module is tested using synthetic data. The estimated planar L2 norm errors obtained from the numerical validation is less than 1% temperatures and less than 2% for soot volume fractions.

OH Emission Intensity Module

The last module developed is the OH emission intensity module. For OH emission intensities, the local intensities are obtained by assuming that self-absorption is negligible. With this thin media approximation, Eq. (7) for the OH intensities can be approximated as:

$$I_\lambda^i = \sum_{k=1}^{N} I_{b\lambda}^k .[1 - \exp(\alpha_{k\lambda} . \Delta_k)] \tag{10}$$

where α is the absorption coefficient of OH. The absorption coefficient of OH that is available from HITRAN is used for the Phase I work. It should be noted that the self-absorption of the radiation due to the OH can be neglected only in non-sooting flames. This module estimates OH concentrations from emission tomography at 310 nm. The data to populate the absorption coefficients of OH are available from HITRAN online. These three modules are used in a SQL database so that any of these modules can be chosen with the appropriate receiving and sending module.

Results and Discussion

The first demonstration experiment is the estimation of the soot volume fraction in the overfire region of turbulent propylene and ethylene diffusion flames.

Evaluation of Soot Volume Fraction Module

For the first experiment, a 50 mm diameter burner is used. A schematic and a photo of the 50 mm diameter burner used for the demonstration tests are shown in Fig. 5. The fuel is introduced at the bottom of the 50 mm ID stainless steel pipe.

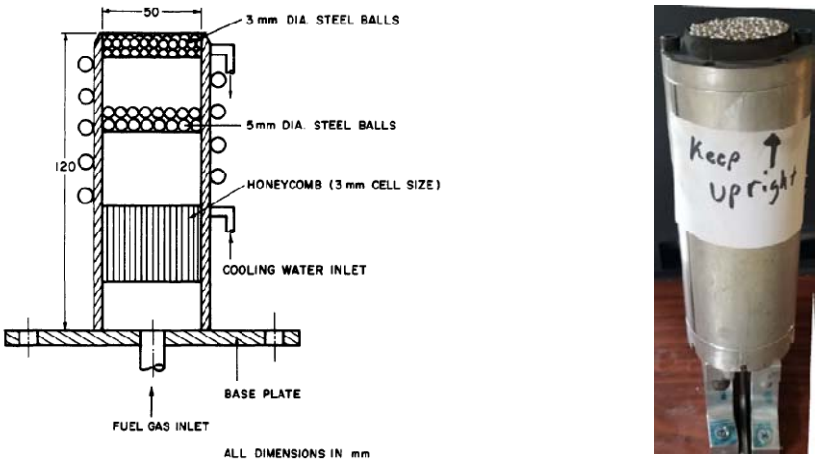

Figure 5. Schematic (left) and photograph (right) of 50 mm diameter burner.

The fuel flow is laminarized using a honeycomb layer followed by two layers of steel balls. The primary advantage of using this burner for the evaluation tests is that published data on soot concentrations in the overfire region, and temperature measurements in the underfire region are available in the literature (Sivathanu, 1990; Sivathanu and Faeth, 1990a, Sivathanu and Faeth, 1990b). The first layer of steel ball has a diameter of 5 mm each, while the second layer has a 3 mm diameter.The whole burner is water-cooled on the outside by wrapping a copper tube around the burner.

A photograph of the sensor suite used to measure the soot volume fraction in the overfire region of the diffusion flames is shown in Fig. 6.

Figure 6. Photograph of the flame (left) and the sensor suite (right) for overfire region.

The measurement plane is 1.5 meters above the burner exit. This is close to the axial location where soot volume fractions are measured in Sivathanu and Faeth (1990a). To ensure that all the soot is

flowing through the measurement plane of 175 mm, a 5-inch diameter duct is used to funnel the soot into the measurement domain. The photograph of the flame is shown on the left panel of Fig. 5. The pipe that is used to capture all the soot particles can be seen in the right panel of Fig. 5. The sensor suite is located very close to the exhaust hood. The right panel also shows the pipe carrying the soot particles and the sensor suite near the exhaust hood.

A contour map of the planar soot volume fraction for the ethylene and propylene flames are shown in Fig. 7. The data above is obtained over a 10-second sampling window. The sensor suite collected the full planar data at a frequency of 1,000 Hz.

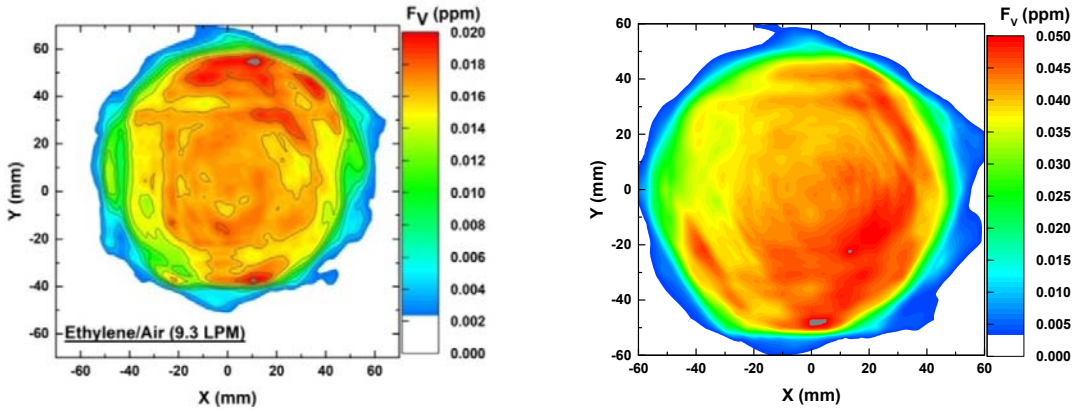

Figure 7. Contour maps of soot volume fraction for ethylene and propylene flames.

The soot volume fractions for the propylene/air diffusion flame are twice that of the ethylene/air diffusion flames, even though the fuel flow rate is lower. This is consistent with past results. These contour maps also show a very close to a uniform distribution with a smaller value close to the edges of the duct. These contour maps are used to find the radial profiles of soot volume fractions. The radial profiles of soot volume fraction for the ethylene and propylene flames are shown in Fig. 8.

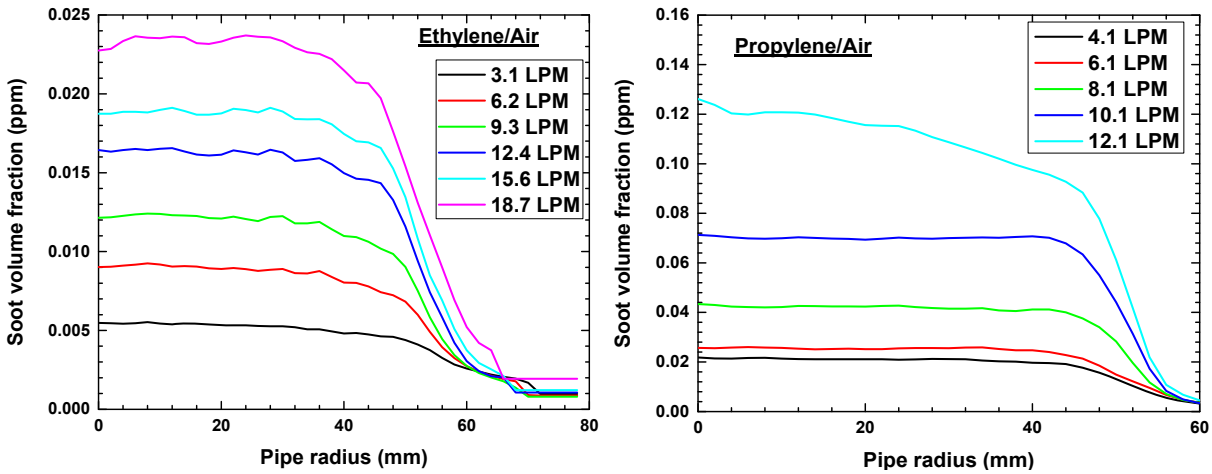

Figure 8. Radial profiles of soot volume fraction estimated from the sensor suite.

Six flow rates of ethylene/air and six flow rates for the propylene/air diffusion flames are used in the experiments. Only 5 of the radial profiles are shown in the propylene/air diffusion flame due to some data corruption with the lowest flow rate condition. The soot volume fractions are nearly constant across the diameter of approximately 50 mm.

Since the soot is all collected and funneled through a pipe, the mixture fraction within the pipe near the measurement zone is uniform. To compare the soot volume fractions with published values, the mixture fraction within the pipe is estimated based on the exhaust velocity and the fuel flow rate.

The mean soot volume fraction (for the first 50 mm diameter in the pipe) as a function of the mixture fraction is shown in Fig. 9. The soot volume fraction state relationship from Sivathanu and Faeth (1990a) for the two fuels are also shown in Fig. 9.

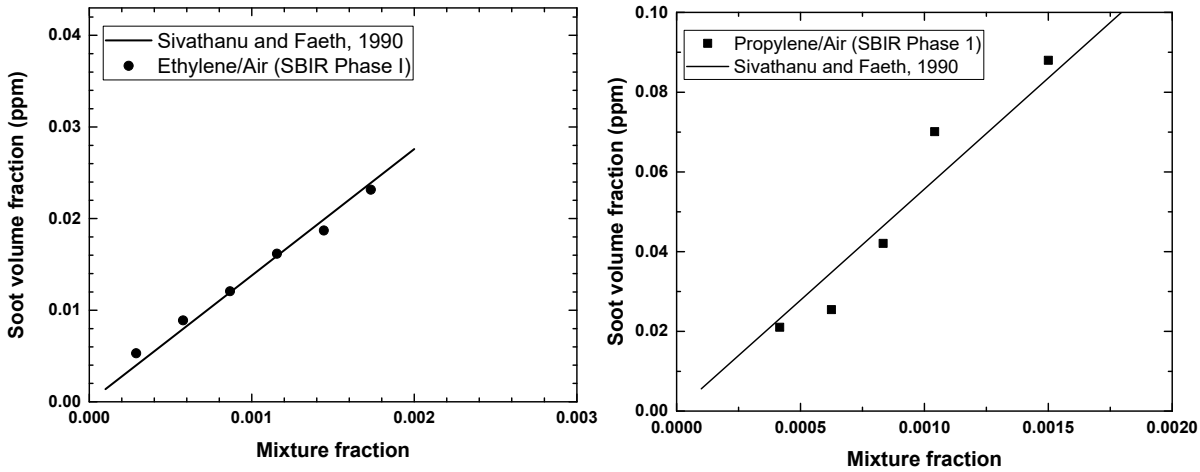

Figure 9. Soot volume fraction state relationship in sooting diffusion flames.

There is a very good agreement between the published values of the soot state relationship and the values obtained from the present experiment. This completely demonstrates the feasibility of using the sensor suite to obtain particulate concentration in the overfire region of turbulent diffusion flames.

Evaluation of Combined Soot Volume Fraction and Temperature Module

The same 50 mm diameter burner is used to obtain temperature and soot volume fraction in the underfire region of the turbulent diffusion flame. The measurements are obtained at an axial height of 100 mm from the burner exit. A photograph of the sensor suite being used for the underfire experiments is shown in Fig. 10.

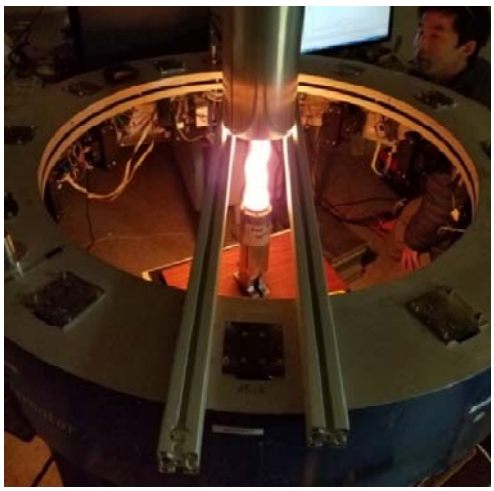

Figure 10. Photograph of the flame and the sensor suite for the underfire region.

The radiation emitted at 800 nm is first obtained for 10 seconds. The 800 nm filters are replaced with 900 nm filters and the radiation obtained for an additional period of 10 seconds. Ideally, the radiation intensities should be obtained at both wavelengths simultaneously so that it can be ensured that the 800 nm and 900 nm data are obtained under identical conditions. Since only six linear arrays are used during this study, the data is collected sequentially. The planar soot volume fraction and temperature obtained at one flow condition for the ethylene/air diffusion flame is shown in Fig. 11.

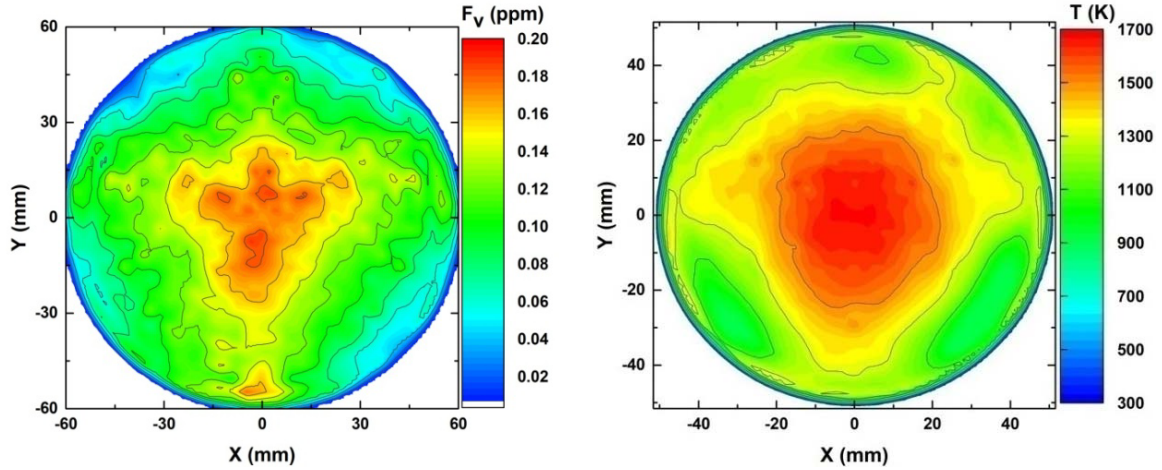

Figure 11. Planar soot volume fractions and temperatures in ethylene/air diffusion flame.

The temperatures range from approximately 700 to 1700 K. Soot volume fractions range from 0.04 ppm to 0.2 ppm. The peak location for temperature and soot volume fraction are similar. These contour maps can be used to obtain radial profiles of soot volume fraction and temperatures in these flames. The radial profiles of soot volume fraction and temperature are shown in Fig. 12.

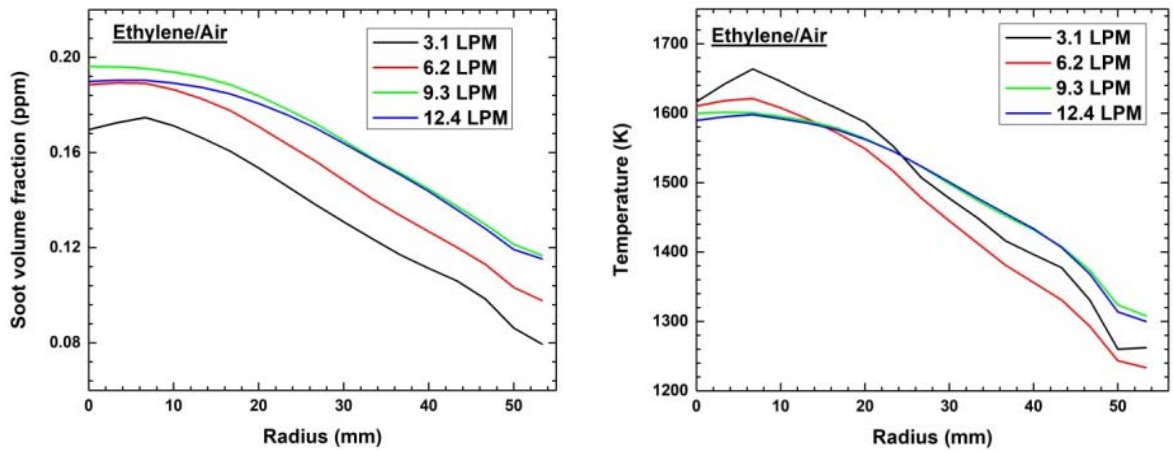

Figure 12. Radial profiles of soot volume fractions and temperatures in ethylene/air flames.

The radial profiles of temperature do not vary much with flow rate to each other. This is expected for the buoyant diffusion flames. The peak temperatures are also similar to what is expected in these flames. The soot volume fractions are also nearly independent of flow rate except at the lowest flow. At the lowest flow rate, the soot volume fraction is slightly lower than at the other conditions. In addition, the peak values of soot volume fractions are lower than those reported in the literature

(Sivathanu and Faeth, 1990b). However, the results reported in the literature are obtained with an intrusive probe and from conditional PDFs. This implies that the soot volume fraction ranged from 0.02 ppm to 2 ppm in the underfire region. For the present measurements, the mean soot volume fraction is 0.20 ppm. There is no comparable data in the literature to verify the mean soot volume fraction data.

The planar soot volume fraction and temperature obtained at one flow condition for the propylene/air diffusion flame is shown in Fig. 13. Qualitatively, the temperatures obtained for the propylene/air diffusion flames are slightly lower than those obtained for the ethylene/air diffusion flames. In addition, the peak soot volume fractions in the propylene/air diffusion flames are marginally higher than those obtained in the ethylene/air diffusion flames.

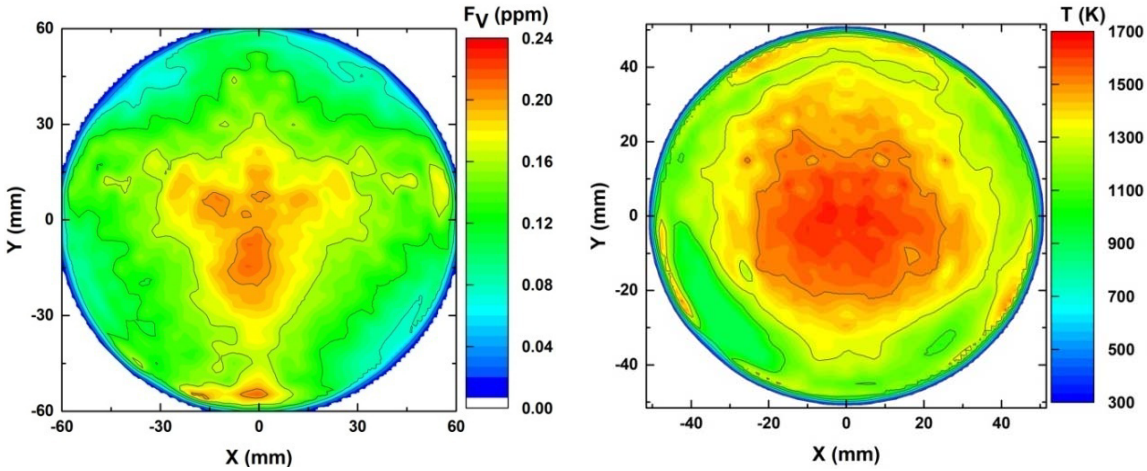

Figure 13. Planar soot volume fractions and temperatures in propylene/air diffusion flame.

The radial profiles of the mean soot volume fractions and temperatures for the propylene/air diffusion flames are shown in Fig. 14.

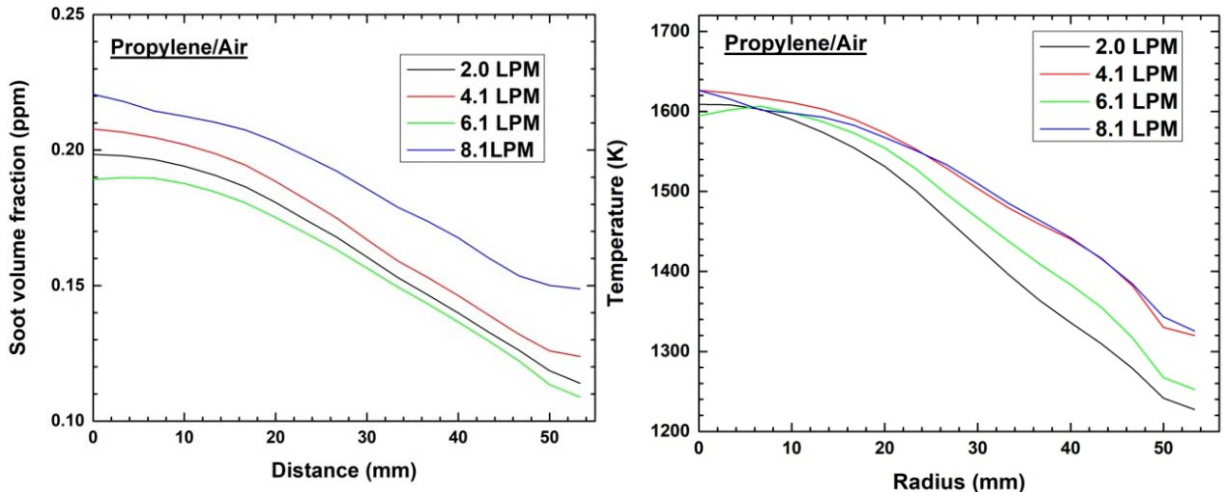

Figure 14. Radial profiles of soot volume fractions and temperatures in propylene/air flames.

The temperature profiles are similar to each other for different flow rates. The soot volume fraction increases with the fuel flow rate. This is consistent with the notion of a constant soot generation efficiency in flames (Koylu et al., 1992). The soot generation efficiencies can be obtained

only in the overfire region after all combustion is complete. The mean temperatures at the centerline are very similar to those obtained with the ethylene/air diffusion flames. The mean soot volume fractions are approximately 25% higher than that of the ethylene/air diffusion flames. This is qualitatively consistent with the literature data. The soot generation efficiencies are approximately 3 times higher for ethylene. The flow rate of fuel is approximately half that of the ethylene/air diffusion flame. In this study, the soot generated is a factor of 2.5 higher for the propylene/air diffusion flames.

Finally, soot temperature correlations are studied for these flames. The mean temperature variation with the mean soot volume faction for ethylene/air and propylene/air diffusion flames is shown in Fig. 15. The soot volume fractions are linearly correlated with the temperature. In addition, this correlation is independent of axial location. This satisfies one of the criteria of the temperature/soot volume fraction state relationship (Sivathanu and Faeth, 1990b.).

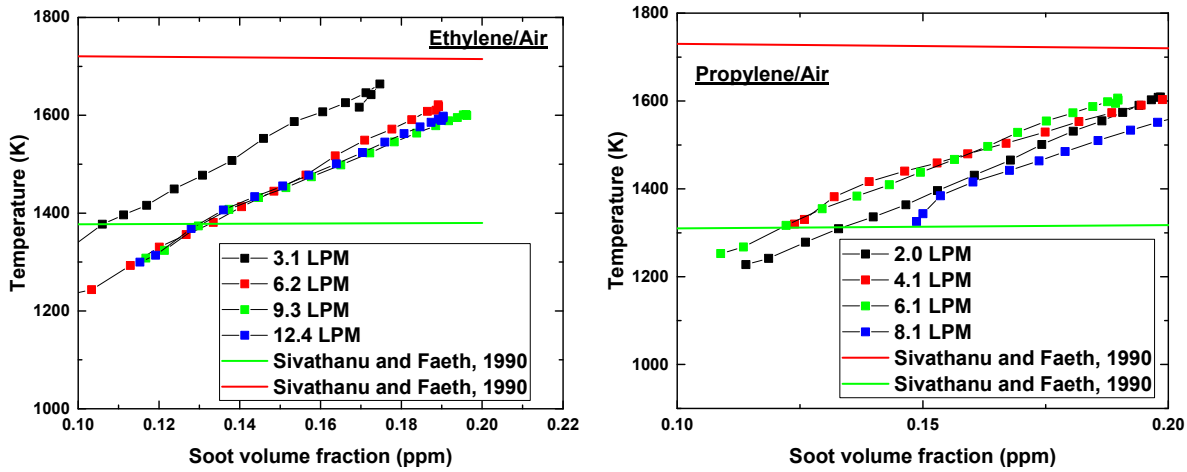

Figure 14. Soot volume fraction/temperature correlations in hydrocarbon flames.

The temperature/soot volume fraction correlation reported in the literature (Sivathanu and Faeth, 1990b) is also shown in Fig. 14. The green line is the mean correlation value - 1σ, and the red line is the mean correlation value + 1σ. The current measurements fall within these values. We found some low-temperature soot values that were not found in the past analysis. Soot at low values and low temperatures are difficult to detect with intrusive probes. The current measurement shows that the temperature increases slightly with the soot volume fraction. Despite these differences, the results obtained thoroughly demonstrate the feasibility of the proposed sensor suite. Furthermore, the quality of the data collected is superior to that obtained using an intrusive probe.

Also, to the time-averaged data, a sample set of emission intensities are obtained from the six receiver modules. This sample set is obtained with three modules at 800 nm and the other three at 900 nm. Since both wavelengths are obtained simultaneously, we can demonstrate the capability of achieving transient temperatures and soot volume fractions within these flames.

The transient temperatures and soot volume fraction obtained from the propylene/air diffusion flame is shown in Fig. 15. The transient radial profiles of temperatures and soot volume fractions for 5 seconds with a temporal resolution of 1,000 Hz is shown in Fig. 15. The temperatures have large fluctuations ranging from 1300 to 1600 K, as expected in turbulent diffusion flames. The soot volume fractions also show a considerable variation with time. The results demonstrate that the modular sensor suite can provide detailed transient temperatures and particulate concentrations in turbulent diffusion flames.

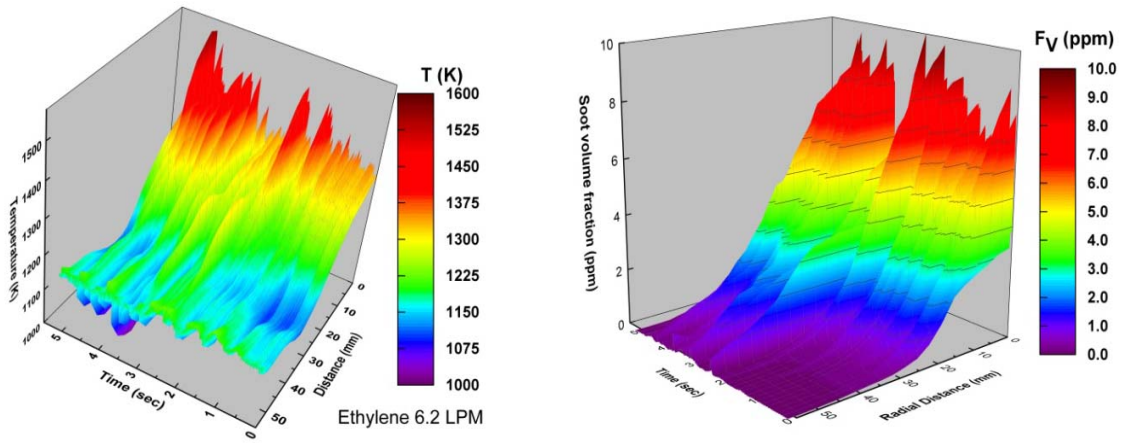

Figure 15. Transient temperatures and soot volume fractions in a propylene/air diffusion flame.

Evaluation of OH emission intensity module

For the third configuration, a turbulent hydrogen/air diffusion flame from a 10 mm diameter burner. A photograph of the experimental arrangement is shown in Fig. 16.

Figure 16. Photograph of the experiment arrangement used for OH emission measurements.

Sample results obtained from the experiment are shown in Fig. 17.

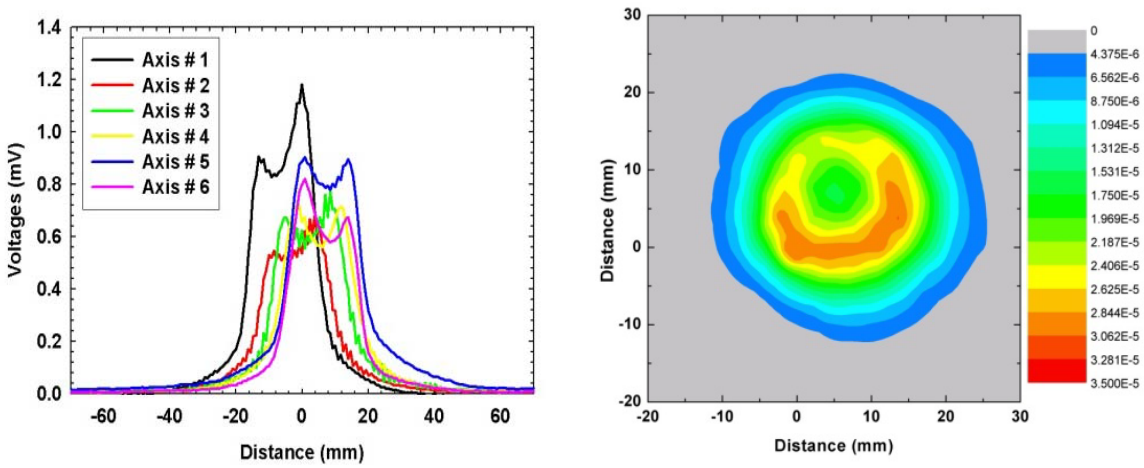

Figure 17. Raw voltages (left) and OH intensities (right) from a hydrogen/air diffusion flame.

For comparison, raw photon counts and OH concentrations in a Hydrogen/Air diffusion flame published recently (Zhao et al., 2018) is shown in Fig. 18.

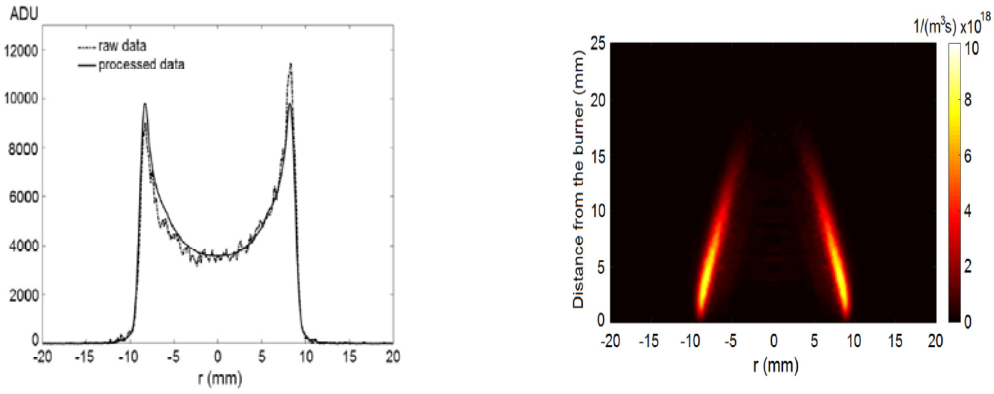

Figure 18. OH emission intensities (left) and concentrations (right) from Zhao et al., 2018.

There is a similar asymmetry in the data provided by Zhao et al. (2018). Besides, the emission intensity at the center is roughly half the peak value. This provides some qualitative validation of the OH emission intensity measurements. However, to get absolute concentrations (quantitative validation), the flame temperature must be input into the module. This data is not available for the hydrogen/air diffusion flame that we used for the experimental validation.

The results show that sensor suite can be used to obtain planar temperatures, soot volume fractions, and radical species emission concentrations in flames.. A long-standing technical hurdle to emission tomography of flames has been broad emission angle detection, rather than line integral detection. Therefore, in front of the linear array detectors, the modular suite uses fiber optic capillary plates to make emission tomography analogous to extinction tomography, at least in terms of the line-integral deconvolution method.

Evaluation of Planar Surface Area Density and Drop Sizes

The last set of experiments are conducted with non-reacting sprays. A photograph of a spray nozzle mounted atop the modular sensor suite is shown in Fig. 19.

Figure 19. A photograph of a spray nozzle being characterized with the sensor suite.

Water is sprayed at several pressures into the center of the modular sensor suite. The sensor suite had six lasers centered at 635 nm in front of them. The path integration extinction and scattering

at 0.5 degrees (narrow- angle) are obtained simultaneously using a 2 x 512 element array in the receiver modules. The fixed wavelength diode laser at 635 nm is used as the source in the sending modules. Mie theory is used to obtain both the planar surface area densities as well as the planar Sauter mean diameter. The primary assumption is that the drop sizes are much larger than the wavelength of light.

An oil burner nozzle is used for the spray. Water at 70 PSI is sprayed downwards into the sensor suite. The nozzle has a nominally solid cone behavior. The measured absorptance and scattered light intensity from the spray are shown in Fig. 20. The absorptance across the six-axis of the modular sensor suite is shown on the left panel of Fig. 20. The peak absorptance at the center of the spray is approximately 0.25. The absorptance profiles are very smooth and equal in all the axis. This profile denotes that the surface area density of the spray is expected to be uniform. The scattered light intensity (as a % of the absorptance) is shown on the right panel of Fig. 20. The scattered intensity is not the same for all the axis. This implies that the drop size distribution within the measurement zone is non-uniform.

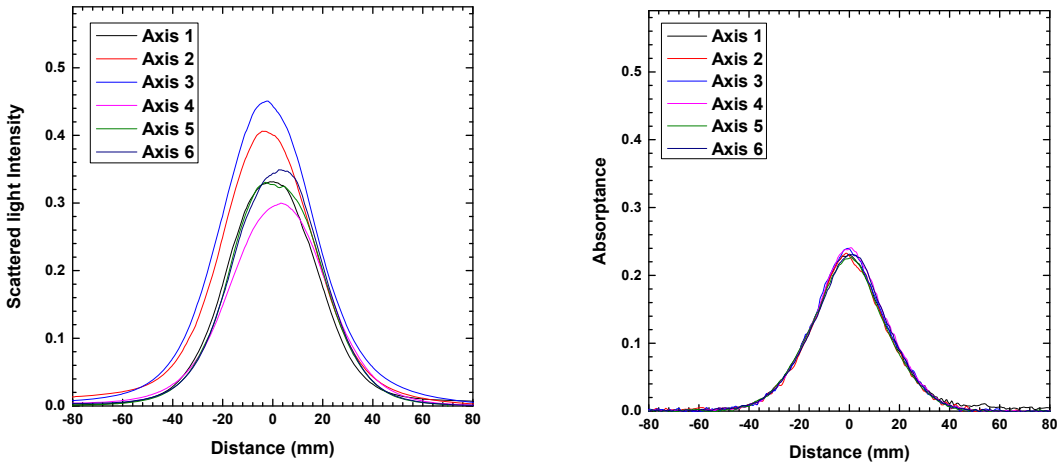

Figure 20. Scattering and absorptance signatures from a water spray.

The deconvolution of the extinction signal provides the planar surface area densities, and the scattering signal's deconvolution provides the planar SMD of the drops.

Contour maps of the planar surface area densities and the planar SMD are shown in Fig. 21.

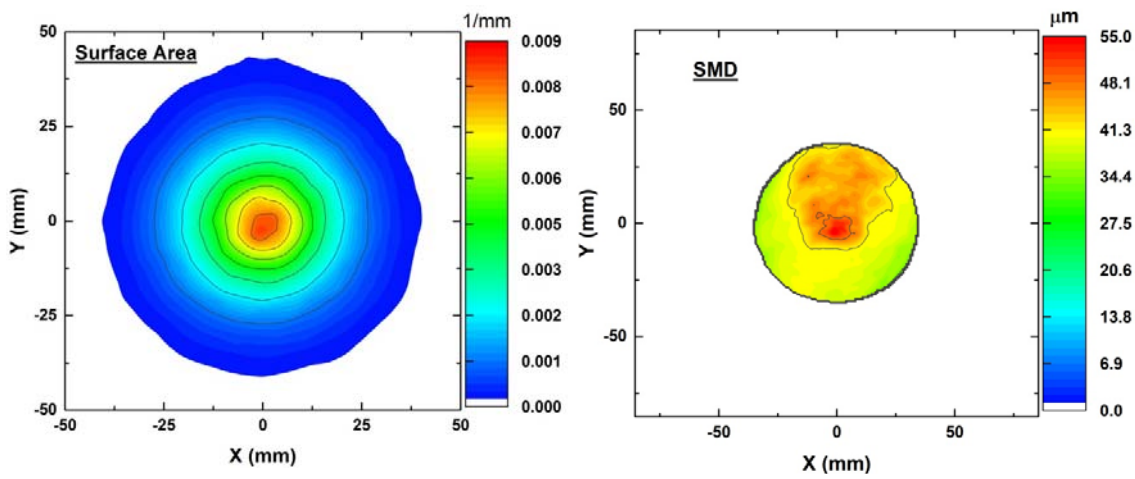

Figure 21. Planar surface area densities and SMD from a water spray.

The surface area density plots are currently used widely by aero-engine nozzle manufacturers around the world for the quality audit of spray angles, spray uniformity, and pattern number. The Planar Sauter Mean diameter obtained from the deconvolution of the scattered intensities is shown on the top right panel. There is more asymmetry in the Sauter Mean Diameter of the spray. These results have also been confirmed using Phase Doppler Anemometer.

Conclusions

These results conclusively demonstrated the technical feasibility of a modular sensor suite for flame and spray diagnostics. The specific conclusions are:

1. The sensor suite estimated the planar soot volume fraction in the overfire region of turbulent hydrocarbon diffusion flames using extinction at 632 nm. The planar soot volume fractions estimated in the are in excellent agreement with the values reported in the literature.
2. The sensor suite measured emission intensity at two wavelengths of 800 and 900 nm in the underfire region of hydrocarbon diffusion flames. These intensities are used to estimate the planar temperature and soot volume fraction in these flames. The estimated planar temperatures and soot volume fractions are in agreement with past measurements.
3. The sensor suite measured the planar OH emission intensities at 310 nm from turbulent H2/O2 diffusion flames. The OH concentration estimates are in qualitative agreement with reported values.
4. The sensor suite used combined scattering and extinction at 635 nm to obtain drop surface areas and drop sizes in a turbulent water spray. The estimated drop size measurements are in agreement with Phase Doppler Interferometry measurements.

Acknowledgement

This work is funded by the National Aeronautics and Space Administration under an SBIR grant with Mr. Glen Guzik acting as the Program Manager.

References

Alkislar MB, Lourenco LM, and Krothapalli A, 2000, ‘‘Stereoscopic PIV Measurements of a Screeching Supersonic Jet," J. Visualization, vol. 3, pp. 135–143.

Bohlin A, and Kliewer CJ, 2014, "Diagnostic imaging in flames with instantaneous planar Coherent Raman Spectroscopy" J. Phys. Chem. Letters, vol. 5, pp. 1243–1248.

Brisley PM, Lu G, Yan Y, and Cornwell S, 2005, "Three-Dimensional Temperature Measurement of Combustion Flames Using a Single Monochromatic CCD Camera," IEEE Transaction on Instrumentation and Measurement, vol. 54, pp. 1417-1421.

Ehn A, Zhu J, Li X, and Kiefer J, 2017, "Advanced laser-based techniques for gas-phase diagnostics in combustion and aerospace engineering," Applied Spectroscopy, vol 7, pp. 341-366.

Floyd J, Geipel P, and Kempf A, 2011, "Computed tomography of Chemiluminescence (CTC): Instantaneous 3D measurements and phantom studies of a turbulent opposed jet flame," Combust. Flame, vol. 2011, pp. 376–391.

Koylu, UO, Sivathanu YR, and Faeth, GM, 1991, "Carbon Monoxide Emissions from Buoyant Turbulent Diffusion Flames," Proceedings of the Third International Symposium on Fire Safety Science, pp. 625-634.

Lim J and Sivathanu Y, 2005, “Optical patternation of a multihole nozzle” Atomization and Sprays, vol. 15, pp. 687-698.

Lim J, Sivathanu Y, Narayanan V, and Seungmin C, 2003, “Optical patternation of a water spray using statistical extinction tomography,” Atomization and Sprays, vol. 13, pp. 27-43.

Seigel R, and Howell JR, 1992, Thermal Radiation Heat Transfer, Hemisphere, Washington DC.

Sivathanu YR, 1990, “Soot and radiation properties of buoyant turbulent diffusion flames,” Ph. D. Thesis, The University of Michigan, Ann Arbor, MI.

Sivathanu YR, and Faeth, GM, 1990a, “Soot Volume Fractions in the Overfire Region of Turbulent Diffusion Flames,” Combust. and Flame, vol. 81, pp. 133-149.

Sivathanu YR, and Faeth GM, 1990b, “Temperature/ soot volume fraction correlations in fuel-rich region of buoyant turbulent diffusion flames,” Combust. Flame, vol. 89, pp. 150-165.

Sivathanu Y, Lim J, Reinhart LE, and Bowman RC, 2007, “Structure of Plumes from Burning Aluminized Propellant Estimated using Fan Beam Emission Tomography,” AIAA Journal, vol. 45, No. 9, pp. 2259-2266.

Sivathanu Y, Lim J, Muliadi A, Nitulescu O, and Shieh T, 2019, "Estimating Velocity in GDI injectors using Statistical Pattern Imaging Velocimetry," International Journal of Spray and Combustion Dynamics, vol. 11, issue 1.

Vardi Y, and Lee D, 1993, “From image deblurring to optimal investments: Maximum Likelihood Solutions for positive linear inverse problems,” J. Statist. Soc. B, vol. 55, pp. 569-612.

Williams TC, Shaddix CR, Jensen KA, Suo-Antilla JM, 2006, "Measurement of dimensionless extinction coefficient of soot within laminar diffusion flames," Combust. Flame, vol. 50, pp. 1616-1630.

Xu L, Liu C, Jing W, Cao Z, Xue X, and Lin Y, 2016, "Tunable diode laser absorption spectroscopy-based tomography system for on-line monitoring of two-dimensional distributions of temperature and H2O mole fraction," Review of Scientific Instruments, vol. 87, p. 013101.

Zhao M, Buttsworth D, and Choudhury R, 2018, "Experimental and numerical study of OH chemiluminescence in hydrogen diffusion flames," Combust. Flame, vol. 197, pp. 369-377.

Zhou B, Brackmann C,Li Q, Wang Z, Petersson P, Li Z, Alden M, and Bai XS, 2015, ‘‘Distributed reactions in highly turbulent premixed Methane/Air flames: Part I. Flame structure characterization’’ Combust. Flame. vol. 162, pp. 2937–2953.